Hindawi
Advances in Meteorology
Volume 2019, Article ID 3148432, 14 pages
https://doi.org/10.1155/2019/3148432

Research Article

Impacts of Chemical and Synoptic Processes on Summer Tropospheric Ozone Trend in North China

Lihua Zhou,[1] **Jing Zhang**,[1] **Xiaohui Zheng**,[2] **Wenhao Xue**,[1] **and Siguang Zhu**[3]

[1]*College of Global Change and Earth System Science, Beijing Normal University, Beijing 100875, China*
[2]*China Meteorological Administration Training Center, CMA, Beijing 100081, China*
[3]*Collaborative Innovation Center on Forecast and Evaluation of Meteorological Disasters/Key Laboratory of Meteorological Disaster of Ministry of Education, Nanjing University of Information Science and Technology, Nanjing 210044, China*

Correspondence should be addressed to Jing Zhang; jingzhang@bnu.edu.cn

Received 24 June 2019; Revised 11 October 2019; Accepted 16 November 2019; Published 29 December 2019

Academic Editor: Nir Y. Krakauer

Compared with other regions in China, air pollution on the North China Plain (NCP) is serious. Fine particle pollution has been studied in-depth, but there is less research on long-term troposphere ozone (O_3) variation. This study focuses on the summer interannual tropospheric O_3 variation on the NCP and its influential factors. Our analysis relies on satellite observations (O_3, nitrogen dioxide (NO_2), sulfur dioxide (SO_2), carbon monoxide (CO), and formaldehyde (HCHO), determined as vertical column density of the troposphere) and dynamical processes (El Niño-Southern Oscillation (ENSO), potential vorticity (PV), the quasibiennial oscillation (QBO), and East Asian summer monsoon index (EASMI)). Our results show the vertical column density of tropospheric O_3 has a transition from the increasing trend to decreasing trend during the summer of 2005–2016. The summer series of tropospheric O_3 show two distinct phases: the first phase (2005–2011), with an average growth rate of 0.55 ± 0.20 DU/yr, and a second phase (2012–2016), with an average reduction rate of 0.16 ± 0.23 DU/yr. The tropospheric NO_2 column in the NCP also has a transition from the increasing trend to decreasing trend during the summer of 2005–2016. Tropospheric NO_2 and CO column concentrations obtained from satellite observations indicate that emission reductions might be the main cause of the tropospheric O_3 decrease. Particularly, the reduction of nitrogen oxides (NO_x) is more significant, and NO_2 decreased by $(0.45 \pm 0.11) \times 10^{15}$ molec·cm^{-2} per year in summer since 2012. However, tropospheric column HCHO shows an increase of 0.05×10^{15} molec·cm^{-2} per year during the whole period of 2005 to 2016. An O_3-NO_x-VOC sensitivity experiment in the NCP showed that the O_3 is still in a NO_x-saturated state in some heavily polluted cities, although the NO_x emissions are decreasing overall. In addition to the chemical reactions, atmospheric dynamic processes also have an effect on tropospheric O_3. Finally, we built a model to analyze the contributions of chemical processes and dynamic processes to the tropospheric O_3 column in the NCP. For the chemical process variables, 69.73% of the observed trend of tropospheric O_3 could be explained by the NO_2 tropospheric column. Therefore, the reduction of tropospheric O_3 since 2012 is associated with the reduction of NOx. For the dynamical process variables, ENSO, PV, and EASMI can explain 60.64% of the observed trend of tropospheric O_3. This result indicates that the atmospheric circulation of the western Pacific Ocean in summer has a significant impact on the interannual trends of tropospheric O_3 in the NCP. It is also found that chemical processes had a more important impact on interannual tropospheric O_3 than dynamic processes, although the dynamic processes cannot be neglected.

1. Introduction

Atmospheric ozone (O_3) is mostly found within the stratosphere, and tropospheric O_3 is approximately one-tenth of the atmospheric column O_3 [1]. However, tropospheric O_3 has direct and detrimental impacts on ecosystems [2, 3]. The production of tropospheric O_3 is chemically controlled by the nonlinear relationship of its precursors, volatile organic compounds (VOCs), and nitrogen oxides (NO_x), implying the complexity of the O_3 pollution. The temporal and spatial

changes of tropospheric O_3 are also controlled by meteorological conditions [1].

Urban agglomerations in China have been experiencing O_3 pollution in recent years. The Yangtze River Delta (YRD) is one of the regions experiencing serious O_3 pollution, with the highest frequency occurring in late spring and early summer [4]. The Pearl River Delta (PRD) is another region with serious O_3 pollution [5]. The NCP has not only been suffering from severe hazy weather but is also one of the regions with serious O_3 pollution in summer [6–8]. It was reported that O_3 pollution episodes reached 286 ppbv (1-h O_3 = 286 ppbv) observed on June 30, 2005, in mountainous areas of north Beijing [9]. In the PRD, surface O_3 increased by 0.86 ppbv/year from 2006 to 2011 [10]. In the NCP, aircraft data indicated a boundary-layer O_3 increase of 2%/year in the summer time during 1995–2005; the surface daily 1-hour maximum O_3 in urban Beijing increased by 1.3%/year during 2001–2006 [11], and the daily 8-hour maximum O_3 in rural Beijing (Shangdianzi) increased at a rate of 1.1 ppbv/year during 2003–2015 [12]. However, due to the environmental protection regulations in China, emissions of precursor NO have decreased since 2011 and 2012. For 2010 and 2014, NO emissions were 1.6 and 1.5 Gg/d in the PRD, 3.9 and 3.0 Gg/d in the YRD, and 15.6 and 14.3 Gg/d in the NCP, respectively. Model and OMI HCHO data show the uptrends in East Asia resulting from anthropogenic activities in China during the last decade and future [13, 14]; however, the trends are negative in the PRD. Much work has been done via case studies of the O_3–VOC–NO_x system sensitivity [15]. Areas around the Bohai Sea became more NO saturated [16]. However, the long-term trend of O_3 is less noticed and studied. Most of the research on O_3 in the NCP was based on model simulations and short-term site observations [17–19] and lacks long-term sequence presentation. Research on long-term changes in O_3 pollution is very limited due to scarce ground observations.

In this study, O_3 long-term variations are investigated based on atmospheric compositions obtained from satellite observations. In recent years, satellite data have been used to study air pollutants [20, 21]. Atmospheric environmental satellite loads have nadir and limb scan modes. Limb mode instruments provide vertical column density and vertical profile data. The Scanning Imaging Absorption Spectrometer for Atmospheric Chartography (SCIAMACHY) has three different viewing geometries: nadir, limb, and sun/moon occultations. Tropospheric Emission Spectrometer (TES) operates in a combination of limb and nadir mode. The Ozone Monitoring Instrument (OMI), Measurement of Pollution in the Troposphere (MOPITT), and Total Ozone Monitoring Spectrometer (TOMS) are nadir instruments and provide total vertical column (O_3, SO_2, NO_2, HCHO, CO, and CH_4). These data have been used to study air pollution [22], and a little research on greenhouse gases has also been involved [23]. Satellite data of column density for SO_2, NO_2, and CO are often used to study air pollution directly. Many studies indicated that OMI observations are credible for assessments of regional and global characterizations of NO_2 and SO_2 spatiotemporal variability [24–26]. However, due to the particular characteristics of the vertical distribution of O_3 (the peak in the stratosphere), it is not appropriate to use the total amount of the nadir column data alone. The nadir observation instrument OMI can obtain the O_3 vertical column concentration of the whole atmosphere, and the limb observation instrument Microwave Limb Sounder (MLS) can obtain the vertical distribution information of O_3. The tropospheric vertical column O_3 can be obtained by combining the two instruments, which is the OMI/MLS satellite tropospheric O_3 [27, 28]. The temporal and spatial distributions of trace gases are also discussed based on satellite.

Ozone-NO_x-VOC sensitivity and explicative variables of chemical and dynamic processes are discussed in this study. The atmospheric circulation system parameters affecting the weather in China are used to measure the impact of meteorological conditions, such as ENSO, PV, QBO, and EASMI.

Descriptions of satellite observational data, meteorological data, and methods related are presented in Section 2. Section 3 presents the evaluation of the OMI/MLS tropospheric O_3 interannual summer variation and trends of tropospheric O_3 and trends of relevant trace gases and ozone-NO_x-VOC sensitivity. Especially, Section 3.5 shows the summer O_3 fraction of explained variation with respect to the two issues listed above (emissions and meteorological conditions). Finally, the conclusions are summarized in Section 4.

2. Materials and Methodology

2.1. Satellite Data and Methods. Tropospheric O_3 data are obtained from combined observations of two satellite instruments, the Ozone Monitoring Instrument (OMI) and Microwave Limb Sounder (MLS). Daily OMI/MLS tropospheric O_3 data were obtained by subtracting MLS stratospheric column O_3 from OMI total column O_3. Stratospheric column O_3 from MLS was spatially interpolated each day to infill the actual along-track measurements. The monthly means were then determined by averaging all available daily data within each month. The spatial resolution of the data files is $1^\circ \times 1.25^\circ$ (latitude × longitude) (https://acdext.gsfc.nasa.gov/Data_services/cloud_slice/new_data.html) [29, 30].

Daily SO_2 and NO_2 and monthly HCHO data are from the OMI aboard the EOS Aura spacecraft, which was launched on July 15, 2004. The NO_2 tropospheric vertical column densities (cloud-screened at 30%) are from the OMI Level 3 daily global products with a spatial resolution of $0.25^\circ \times 0.25^\circ$. The NO_2 slant column is retrieved in the spectral range of 405–465 nm with a fitting error of $0.3–1 \times 10^{15}$ cm^{-2} before the row anomaly. The noise plumes from strong anthropogenic sources of SO_2 (such as smelters and coal burning power plants) and from strong regional pollution can be detected in scene data. The noise standard deviation (sigma) of vertical column SO_2 data products is about 0.4 DU (1 DU = 2.69×10^{16} molec·cm^{-2}) and decreases with an increasing average number of scenes. The monthly values of NO_2 and SO_2 are calculated from the daily average. Detailed data descriptions are provided in the references [31–34].

The daily total column CO is retrieved from the Measurement of Pollution in the Troposphere (MOPITT) available at https://terra.nasa.gov/about/terra-instruments/mopitt [35]. Its resolution is $1^\circ \times 1^\circ$. In our analysis, the missing values are eliminated. MOPITT's spatial resolution is 22 km at nadir, and its swaths are 640 km wide. Moreover, it can measure the concentrations of CO in 5 km layers down a vertical column of atmosphere. The satellite is deployed in a polar Sun-synchronous orbit with a 10 : 30 local equator crossover time. Retrieved CO total column day data were applied in the study. The MOPITT observations reported here are version 3 data, which have a 10% precision on both column and mixing ratio.

To find the inflection point of the time series, we perform quadratic (second-order polynomial) nonlinear regression. The normal calculation formula is as follows:

$$y(i) = a_1 t(i)^2 + a_2 t(i) + a_3 + \varepsilon(i), \quad (1)$$

where a_1 and a_2 are fitting coefficients, a_3 is the intercept, $t(i)$ is the time index, $\varepsilon(i)$ is the error term, i is the time index, and $y(i)$ are the annual pollutant variables (NO_2, HCHO, SO_2, CO) in summer.

Based on long-term observation data, we first examined long-term interannual variations of O_3 concentrations in the NCP during 2005–2016. We use the linear regression equation to calculate the growth trends of O_3 and pollution gas emissions and divide time into two phases (according to O_3 trend variation). The results are shown in Table 1. The linear regression equation is

$$y(i) = ax(i) + b + \varepsilon(i), \quad (2)$$

where a is the slope from time-series calculation, b is the corresponding intercept, and $\varepsilon(i)$ is the error term.

2.2. Dynamical Variables and Regression Model. Figure 1 shows the study area, which is the NCP. Summer (June, July, and August, i.e., JJA) was selected as the study period.

The considered NCP domain ranges between 34.5°N and 42.5°N in latitude and between 110.5°E and 120.5°E in longitude (Figure 1). The BTT domain ranges between 38.5°N and 40.5°N in latitude and from 115.5°E to 119.0°E in longitude (Figure 1). The other representative cities in the NCP include Shijiazhuang, Jinan, Taiyuan, and Chengde, the city center of which is located within the domain. Annual summer concentrations are obtained based on the regional averages of monthly concentrations calculated from the daily averages. Then, we have standardized (i.e., normalized) NO_2 and HCHO concentrations and meteorological parameters.

A multiple linear regression model was established to assess the contribution of each parameter, as described in the literature [36]:

$$O_3(i) = a_0 i + \sum_{1}^{j} a_j x_j(i) + b + \varepsilon(i), \quad (3)$$

$$R^2_{\text{adjusted}} = 1 - \frac{(1 - R^2)(n-1)}{n - p - 1}, \quad (4)$$

where O_3 is the summer monthly mean troposphere O_3, a_0 is the slope calculated based on regional time series, i is the time index, x_j is the regularized time series parameter, a_j is the corresponding fitting coefficient, and b is the intercept. $\varepsilon(i)$ is the error term. R^2 is R squared goodness of fit. R^2_{adjusted} is adjusted R square. n is the number of samples. p is the number of parameters. Fraction of explained variation is the adjusted R squared of the multivariate regression model (explained variance/total variance). When a meaningful variable is added, adjusted R square will increase. We consider a 95% confidence range ($P < 0.05$ is considered to be significant). The standardization method used in this study involved normalizing to (0, 100) [37]. The standardized parameters are calculated by the following formula:

$$c' = \frac{c_i - c_{\min}}{c_{\max} - c_{\min}} \cdot 100\%, \quad (5)$$

where c' is the normalized time series parameter and $c_{\min}$ and $c_{\max}$ are the minimum and maximum values in the series, respectively [38].

Some large-scale dynamics influence the tropospheric O_3 such as the quasibiennial oscillation (QBO) and the El Niño-Southern Oscillation (ENSO) related to the dynamical processes leading to a modulation of the stratospheric circulation and of the stratospheric-tropospheric exchanges (STE). EASM affects the horizontal transmission of tropospheric O_3. To study the impacts of atmospheric dynamics on tropospheric O_3, several atmospheric circulation factors have also been taken into account, as described below.

The QBO data at 10 hPa (QBO10) and 30 hPa (QBO30) were taken from http://www.geo.fu-berlin.de/met/ag/strat/produkte/qbo/singapore.dat. The QBO dataset adopted has been produced since 1987 from the Singapore data (monthly mean zonal wind components at Singapore, 1N/104E) by using the daily vertical wind profiles to obtain a higher vertical resolution. The time period used in this article is from the summer of 2005 to 2016 (June to August), and the other parameters are in the same period. The multivariate ENSO index (MEI) was taken from https://www.esrl.noaa.gov/psd/enso/mei/table.html. The bimonthly multivariate El Niño/Southern Oscillation (ENSO) index is the time series of the leading combined Empirical Orthogonal Function (EOF) of five different variables (sea level pressure (SLP), sea surface temperature (SST), zonal and meridional components of the surface wind, and outgoing longwave radiation (OLR)) over the tropical Pacific basin (30°S-30°N and 100°E–70°W). The Nino index was from https://http://www.esrl.noaa.gov/psd/gcos_wgsp/Timeseries/Nino34/. The East Asian summer monsoon (EASM) index is defined as an area-averaged seasonally (JJA) dynamical normalized seasonality at 850 hPa within the East Asian monsoon domain (10°–40°N, 110°–140°E) [39–41]. The data were taken from http://ljp.gcess.cn/dct/page/65577. The QBO, ENSO, Nino indices, and EASM are all monthly data. The tropopause height is characterized by the potential vorticity at 300 hPa. These parameters were taken from the ERA-Interim reanalysis at http://apps.ecmwf.int/datasets/data/interim-full-daily/.

Table 1: Annual variation rates of O_3 and other air pollutants from satellite observations over three periods (2005–2011, 2012–2016, and 2005–2016) in the NCP.

		2005–2011	2012–2016	2005–2016
O_3	Variation rate ($DU \cdot yr^{-1}$)	0.55 ± 0.20	-0.16 ± 0.23	0.36 ± 0.09
	r^2	0.60	0.14	0.63
NO_2	Variation rate (10^{15} molec$\cdot cm^{-2} \cdot yr^{-1}$)	0.25 ± 0.05	-0.45 ± 0.11	-0.02 ± 0.05
	r^2	0.85	0.85	0.01
HCHO	Variation rate (10^{15} molec$\cdot cm^{-2} \cdot yr^{-1}$)	0.24 ± 0.11	-0.19 ± 0.32	0.05 ± 0.07
	r^2	0.49	0.11	0.05
CO	Variation rate (10^{18} molec$\cdot cm^{-2} \cdot yr^{-1}$)	-0.03 ± 0.03	-0.05 ± 0.05	-0.02 ± 0.01
	r^2	0.15	0.24	0.26
SO_2	Variation rate ($DU \cdot yr^{-1}$)	0.01 ± 0.02	-0.05 ± 0.00	-0.03 ± 0.01
	r^2	0.06	0.99	0.50

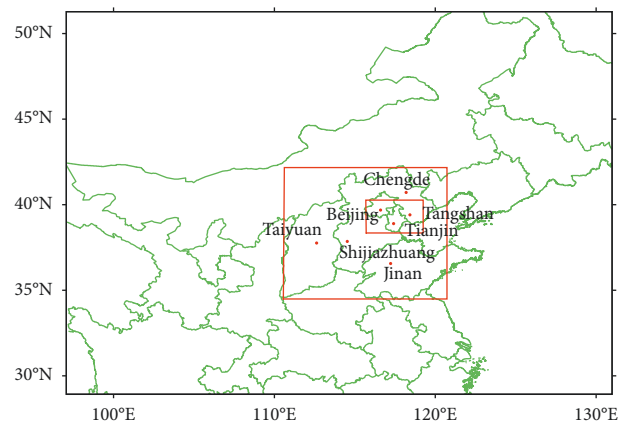

Figure 1: Location of the study area, NCP (outer rectangular area). The main cities considered are Beijing-Tianjin-Tangshan (BTT, inner rectangular area), Taiyuan (TY), Shijiazhuang (SJZ), Jinan (JN), and Chengde (CD).

2.3. Ozone-NO_x-VOC Sensitivity. The formaldehyde nitrogen ratio (FNR) has been used to indicate spatially and temporally heterogeneous ozone-NO_x-VOC sensitivity [42]. FNR is defined as the ratio of tropospheric HCHO column concentration to the NO_2 column concentration and is used here to study the ozone-NO_x-VOC sensitivity in the NCP:

$$\mathrm{FNR} = \frac{\mathrm{column}_{\mathrm{HCHO}}}{\mathrm{column}_{\mathrm{NO_2}}}. \quad (6)$$

The HCHO and NO_2 column concentrations retrieved from the Ozone Monitoring Instrument (OMI) aboard the NASA Aura satellite were used to calculate FNR during the O_3 season. Based on previous experience, the O_3 production regime is thought as VOC-limited if FNR < 1.0, NO_x-limited if FNR > 2.0, and transitional (either NO_x changes or VOC changes would be expected to change O_3 in this interval) if $1.0 < \mathrm{FNR} < 2.0$ [43].

2.4. Evaluation Data. The World Ozone and Ultraviolet Data Center (WOUDC) ozonesonde provides an independent approach of ground observations of tropospheric O_3 and is used here to evaluate the OMI/MLS tropospheric O_3. Another independent tropospheric O_3 observation is balloon radiosonde via an electrochemical concentration cell (ECC-Ozone Sensor) in Beijing (39.80°N, 116.47°E) during April to May 2005, and this approach is also used in this paper for evaluation of the OMI/MLS tropospheric O_3.

3. Results and Discussion

3.1. Evaluation of the OMI/MLS Tropospheric O_3. Column O_3 (CO, in Dobson Units, DU) was determined by standard log-pressure integration of O_3 partial pressure: $\mathrm{CO} = 0.79 \int_{P_1}^{P_2} \mathrm{XP} \cdot \mathrm{DlnP}$, where X is O_3 volume mixing ratio in unit parts per million by volume (ppmv) and P is pressure in units hPa. The satellite and sondes are for a tropospheric average. Tropospheric O_3 is the entire column in the troposphere [29, 30]. The validation is from OMI/MLS and ozonesonde monthly data. The correlation coefficient R between OMI/MLS tropospheric O_3 and WOUDC ozonesonde tropospheric O_3 is 0.936 for ozonesonde station locations lying between 25°S and 50°N, and the Root Mean Square Error (RMSE) is 3.18 ppbv. The deviation is smaller in the lower latitudes. This result also indicates closely similar signatures for seasonal cycles and spatial variability from the comparisons of OMI/MLS tropospheric O_3 between the climatology and other data products [44]. Comparisons with Beijing (39.80°N, 116.47°E) ozonesonde data during April to May 2005 show a typical error of ±10%. If there are enough samples, it will be more convincing.

3.2. Interannual Summer Variation and Trends of Tropospheric O_3. Figure 2 shows the monthly tropospheric O_3 distributions for the study area from 2005 to 2016. The tropospheric O_3 levels are lowest in winter (December/January) and highest in summer (June to August). Spring and autumn are transitional periods. The peak monthly O_3 occurred in June/July. This pattern is consistent with the seasonal variations of temperature and solar radiation. The tropospheric O_3 levels in July increased from 2005 to 2016 at an average rate of 0.2 DU per year, while no such apparent trend is found in winter. The lowest O_3 levels generally occur in January. For instance, the lowest O_3 level during this period occurred in January 2006, which accounted for only 5.65% of the accumulated monthly O_3 of 2006. Similar low values are often recorded in the period of December to February; for example, the O_3 levels in February 2012 and December 2015 accounted for 5.50% and 5.87% of the

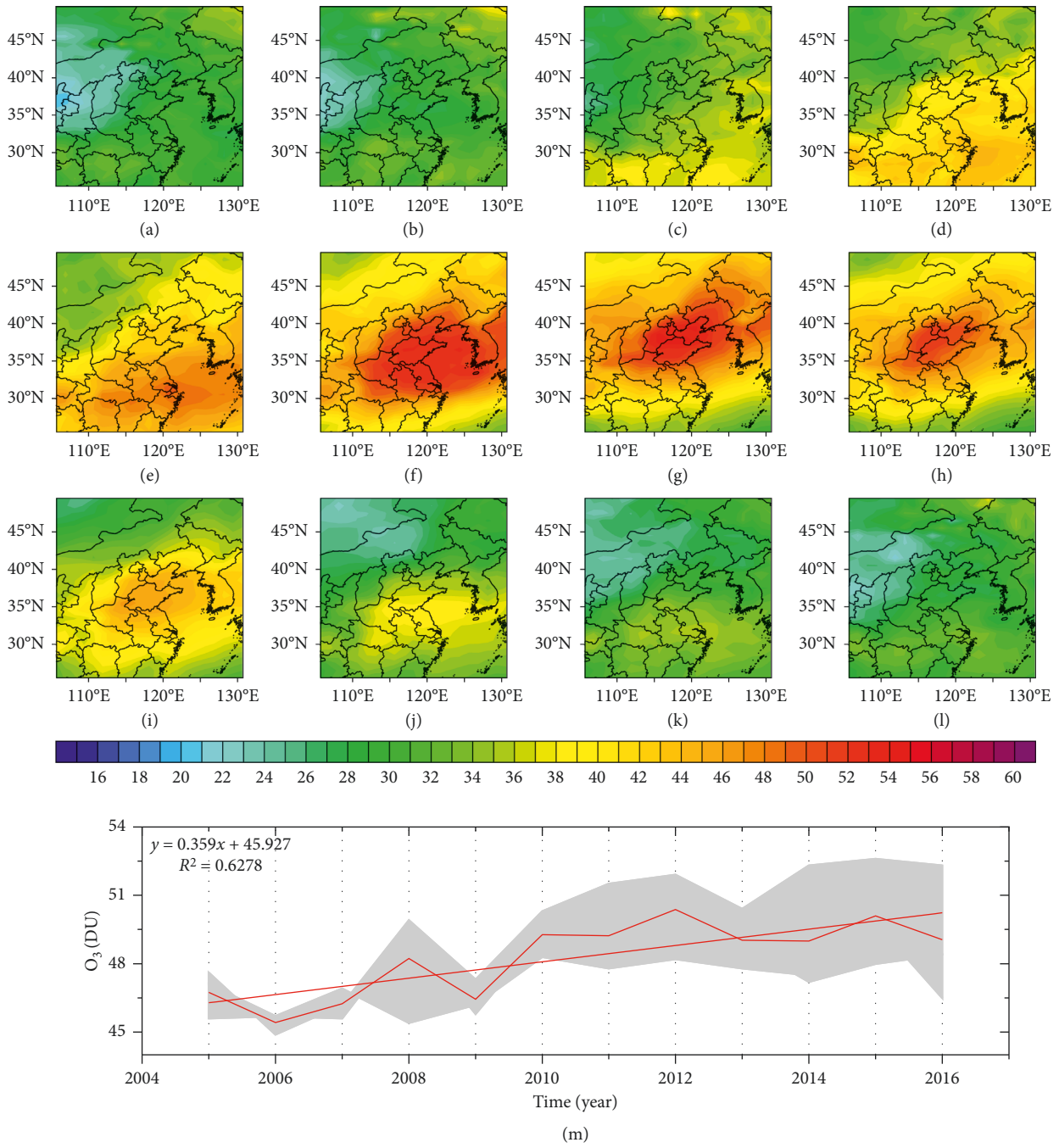

FIGURE 2: Monthly average tropospheric O_3 vertical column density (VCD) (units: DU) during 2005–2016: (a) January; (b) February; (c) March; (d) April; (e) May; (f) June; (g) July; (h) August; (i) September; (j) October; (k) November; (l) December; (m) summer time O_3 series in the NCP, indicated as the area in the outer box in Figure 1. The gray shaded area indicates the variation range because the annual summer data cover 3 months (June to August), and the red line is the summer average of the year.

accumulated monthly O_3, respectively. In contrast, the O_3 level in July 2016 accounted for 11.91% of the O_3 levels for the whole year. Because of the increase in O_3 pollution incidents in North China that occurs during most summers, we focus on the situation of the summer period. The summer time series (Figure 2) have shown that the trend of tropospheric O_3 is increasing with an average rate of 0.36 ± 0.09 DU/yr over 2005–2016. However, the summer tropospheric O_3 column in the NCP has a transition from the increasing trend to decreasing trend over 2005–2016. The tropospheric O_3 trend shows two distinct phases: the first phase (2005–2011), with an average increase rate of 0.55 ± 0.20 DU/yr, and the second phase (2012–2016), with an average decrease rate of 0.16 ± 0.23 DU/yr. The decrease in the tropospheric O_3 in the latter phase might be caused by the emission reductions in recent years. To investigate the impacts of trace

gases on tropospheric O_3, tropospheric column concentrations of several trace gases and meteorological factors are discussed in Section 3.2.

3.3. Interannual Summer Variation and Trends of Relevant Trace Gases. The atmospheric nitrogen oxides (NO_x, including NO and NO_2) are important air pollutants and among the O_3 precursors [45, 46]. Previous studies showed that there is generally a positive correlation between atmospheric NO_x and O_3 concentrations [47].

According to satellite observations, NO_2 pollution in North China is more serious than in adjacent areas [48]. This is generally attributed to the northern industrial areas. Annual averages of tropospheric NO_2 for summer months are shown in Figure 3. Over these 12 years, tropospheric NO_2 peaked in 2011 and 2012, reaching 6.97×10^{15} molec·cm^{-2} in June, 6.15×10^{15} molec·cm^{-2} in July, and 6.14×10^{15} molec·cm^{-2} in August. NO_2 concentrations showed a downward trend from 2011/2012 to 2016. Two phases are discerned: the first phase (2005–2011), with an average increase rate of $(0.25 \pm 0.05) \times 10^{15}$ molec·cm^{-2}·yr^{-1}, and the second phase (2012–2016), with an average decrease rate of $(-0.45 \pm 0.11) \times 10^{15}$ molec·cm^{-2}·yr^{-1}. For the whole period (2005–2016), the NO_2 concentrations decreased at $(-0.02 \pm 0.05) \times 10^{15}$ molec·cm^{-2}·yr^{-1}. In terms of spatial distribution, the NO_2 concentration in urban areas is higher than that in suburbs. Especially in the Beijing-Tianjin-Tangshan area, the NO_2 concentration was extremely high over this period. This result suggests that the BTT area might probably have been in the NO-saturated regime, which is consistent with Souri et al. [16]. Further ozone-NO_x-VOC sensitivity will be discussed in Section 3.3.

HCHO is produced directly and indirectly from both biogenic and anthropogenic sources. According to the research by Zhu et al. [33], satellite observations of HCHO columns provide emissions of highly reactive volatile organic compounds (HRVOCs). This approach has been used previously in the US to estimate isoprene emissions from vegetation. According to Souri et al., in East Asia, OMI HCHO levels were substantially higher in urban regions than in forested areas, indicating predominant anthropogenic VOC emissions. Its spatial distribution map also proves the pattern (Figure 4). The trends of total HCHO columns from the OMI showed widespread upward trends in eastern China and the majority of enhancements in the northern regions from the HCHO time series in NCP from 2005 to 2016. From the HCHO time series from the OMI, the annual minimum is in winter and the annual maximum is in summer.

HCHO is an important intermediate for VOCs, and VOCs are among the O_3 precursors. Thus, the variability of HCHO could be indicative of the spatiotemporal distributions of reactive VOCs. During the first phase (2005–2011), HCHO in the NCP increased at an average rate of $(0.24 \pm 0.11) \times 10^{15}$ molec·cm^{-2}·yr^{-1}, and during the second phase (2012–2016), HCHO decreased at an average rate of $(0.19 \pm 0.32) \times 10^{15}$ molec·cm^{-2}·yr^{-1}. For the whole period (2005–2016), HCHO increased by $(0.05 \pm 0.07) \times 10^{15}$ molec·cm^{-2}·yr^{-1}.

SO_2 does not typically have a significant impact on O_3, but it can characterize pollution emissions level [49]. The annual trend of summer-time SO_2 in North China is shown in Figure 5(c). Quantitative calculations indicate a decreasing overall trend from 2005 to 2016. In the three months (June–August), the monthly average content of SO_2 decreased by 49.1%, 43.2%, and 43.6%, respectively. For comparison purposes, the analysis of SO_2 is also divided into two phases: the first phase (2005–2011), with an average rate of increase of 0.01 ± 0.02 DU·yr^{-1}, and the second phase (2012–2016), with an average rate of decrease of 0.05 DU·yr^{-1}. For the whole period (2005–2016), SO_2 decreased by 0.03 ± 0.01 DU·per·year. The change in SO_2 in summer proves that the emission reduction is significant once again.

The satellite observations of CO indicate that the spatial distribution of CO is basically similar to those of NO_2 and SO_2, all of which have elevated levels in North China compared with surrounding areas. Considering larger scales, their distribution is similar, while for smaller scales, the distribution is different because the life cycle of NO_2 and SO_2 is indeed much shorter than CO. However, the vertical column densities of CO show a clear interannual downward trend (Figure 5(d)) [50, 51], which is different from the trends of NO_2 and SO_2. During the first phase (2005–2011), CO decreased at an average rate of $(0.03 \pm 0.03) \times 10^{18}$ molec·cm^{-2}·yr^{-1}, and during the second phase (2012–2016), it decreased faster, with an average rate of $(0.05 \pm 0.05) \times 10^{18}$ molec·cm^{-2}·yr^{-1}. For the whole period (2005–2016), CO decreased at an average rate of $(0.02 \pm 0.01) \times 10^{18}$ molec·cm^{-2}·yr^{-1}.

The sink of CO includes diffusion, transport, deposition, and chemical transformation. The diffusion and transport of CO in the atmosphere are controlled by wind speed [52]. Local and short-term O_3 concentrations are indeed most severely affected by VOCs. The study region of this paper is the entire North China region, and CO represents a level of primary emissions to a certain extent. Therefore, the CO variable, due to its long lifetime, is considered to be a proxy for large-scale emission changes that may regionally affect O_3 [53, 54].

3.4. FNR and Ozone-NO_x-VOC Sensitivity. From the perspective of photochemical reactions, tropospheric NO_x and VOCs are precursors that need be considered to elucidate the sensitivity of O_3 production. OMI observations of NO_2 and HCHO column densities were used for the exploration of the sensitivities of surface O_3 pollution to NO_x and VOC emissions over the NCP. However, in general, the vertically integrated column may not represent the near-surface environment. This study attempts to use FNR to assess the sensitivities of tropospheric O_3 to NO_x and VOC emissions over the NCP. NO_x-limited and NO_x-saturated conditions were discerned by FNR thresholds at 90% confidence [55].

FNR may vary in space and time, suggesting that there is a transition between NO_x-limited and NO_x-saturated conditions in space and time. Figure 6 shows the average summer (JJA) FNR in the NCP during 2005–2016. A decrease in average summer FNR is observed for the first phase (2005–2011), and this decrease may be caused by increased

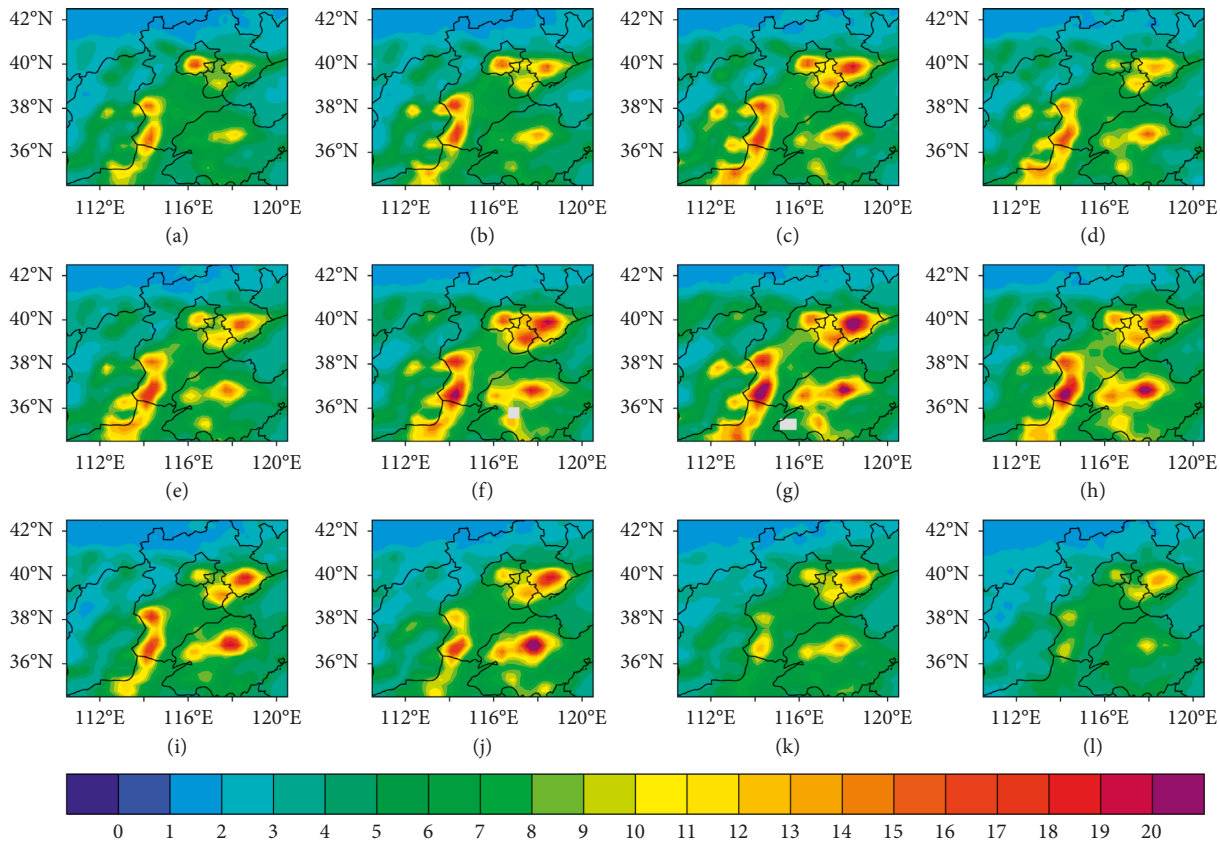

FIGURE 3: Average tropospheric NO_2 vertical column density distribution in summer (JJA) (2005–2016) (units: 10^{15} molec·cm^{-2}): (a) 2005, (b) 2006, (c) 2007, (d) 2008, (e) 2009, (f) 2010, (g) 2011, (h) 2012, (i) 2013, (j) 2014, (k) 2015, and (l) 2016, indicated as the area in the box in Figure 1.

NO_x emissions (with the NO_2 increase rate reaching 0.25 molec·m^{-2}·yr^{-1} (Table 1)). In the urban areas of major cities in the NCP (e.g., BTT, Taiyuan, Shijiazhuang, and Jinan) the summer FNR was extremely low, and this result suggests that in urban areas, O_3 was probably in the NO_x-saturated regime. However, during the second phase (2012–2016), the ratio increased significantly as a result of NOx emission reduction (with a NO_2 decrease rate of −0.45 molec·m^{-2}·yr^{-1} (Table 1)). In representative cities of the NCP, the summer O_3 experienced a transition from the VOC-limited regime to the NOx-limited regime. Away from these urban areas, the summer O_3 had been NO_x-limited.

The regional O_3-NO_x-VOC sensitivities in summer are illustrated by O_3-NO_2-HCHO sensitivities in Figure 7. Generally, higher HCHO would result in higher O_3, while higher NO_2 would or would not, depending on FNR (Figure 7(a)). When the value of FNR is equal to 2, the tropospheric O_3 is close to the vicinity minimum. Therefore, emission reductions of VOCs and NOx are effective for controlling O_3. For the situation with FNR greater than 2 (the area on the right side of line FNR = 2), emission reduction of VOCs is effective for O_3 control, and reduction of NOx may even increase the O_3 concentration. This finding suggests that O_3 is in a NOx -limited regime. For the situation with FNR less than 1 (the area on the left side of line FNR = 1), emission increase of NOx would not effectively increase O_3 concentration, while reduction of VOCs would, thus implying that NOx is oversaturated. For the situation with FNR between 1 and 2 (the area between line FNR = 1 and line FNR = 2), emission reductions of both VOCs and NOx are effective for O_3 control, suggesting that O_3 is in the transition regime. As seen from Figure 6, the FNR was greater than 2 over most areas of the NCP, but in the major metropolitan cities, the FNR was less than 2 and might even have been less than 1 for some years. In these cities, NOx was still saturated for tropospheric O_3 production in the second phase, although their NOx emissions have been decreasing (Figures 3 and 7(b)). Because of the high urban NO_x base level, the emission reduction of NO_x did not result in a distinct O_3 decrease. Overall, the NCP has been experiencing the transition from the NO_x-saturated state to NO_x-limited state by comparison of two time periods (2005–2011 and 2012–2016).

Due to the limitations of the time resolution of satellite observations, the sensitivity experiments we performed did not reflect the continuous variation in a day and daily changes. Because the daily variation of O_3 is relatively large, OMI scanning transit time over NCP is approximately local time 13 : 45, only with once a day [30]. This sensitivity analysis can only reflect the situation of satellite transit time, which is the limitation of this experiment. Another point to note is that tropospheric O_3 is different from the concerned

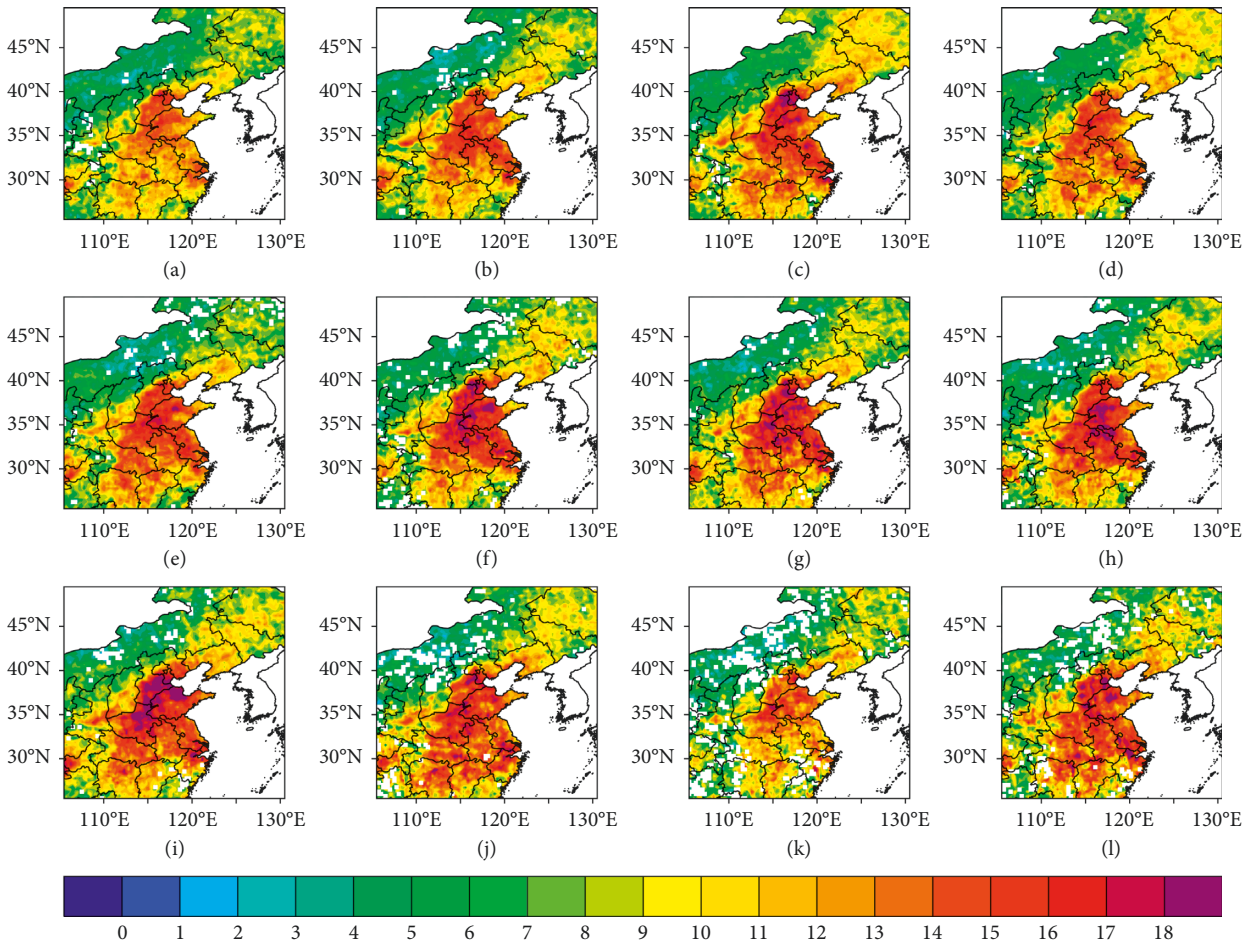

Figure 4: The spatial distribution of HCHO in summer (JJA) is from 2005 to 2016 (units: 10^{18} molec·cm^{-2}). (a) 2005, (b) 2006, (c) 2007, (d) 2008, (e) 2009, (f) 2010, (g) 2011, (h) 2012, (i) 2013, (j) 2014, (k) 2015, and (l) 2016.

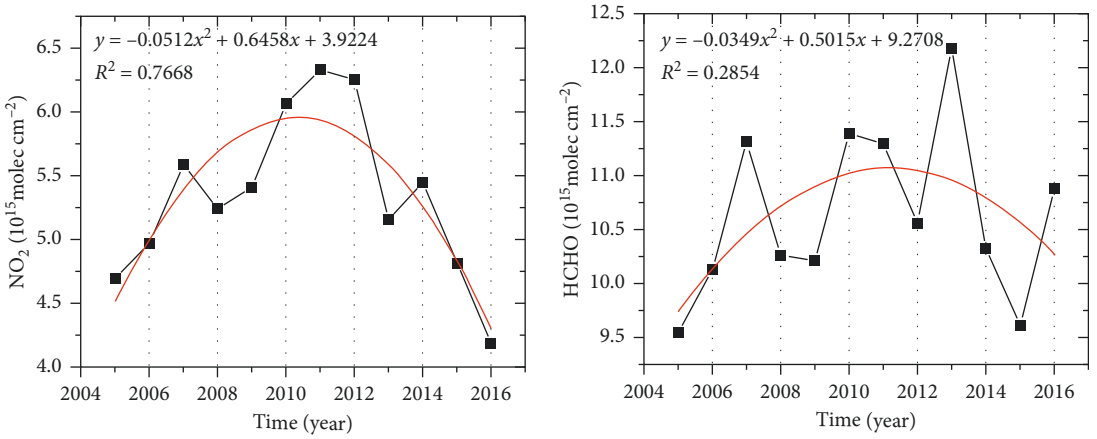

Figure 5: Continued.

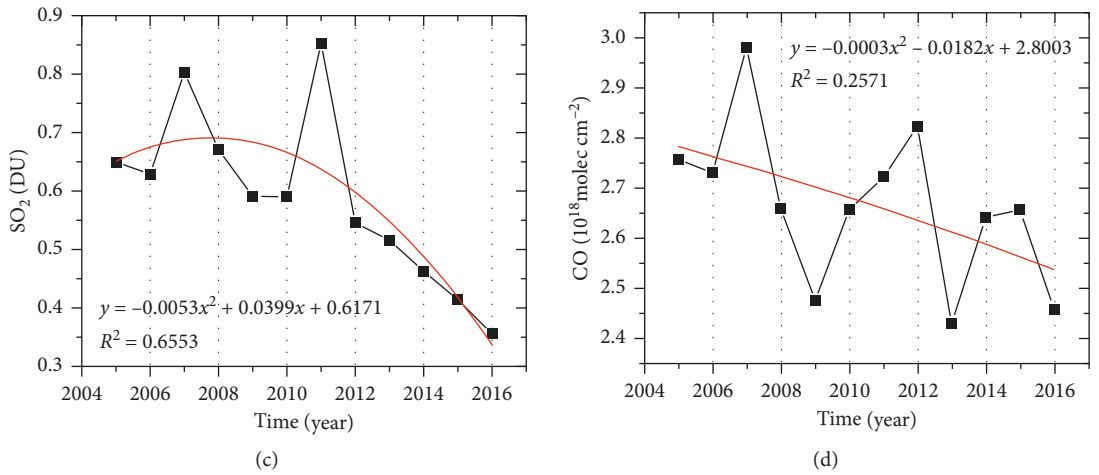

Figure 5: Time series of tropospheric column trace gas concentrations based on satellite observations for each summer during 2005–2016 in the NCP: (a) NO_2, (b) HCHO, (c) SO_2, and (d) CO. Each red line represents the fitting curve.

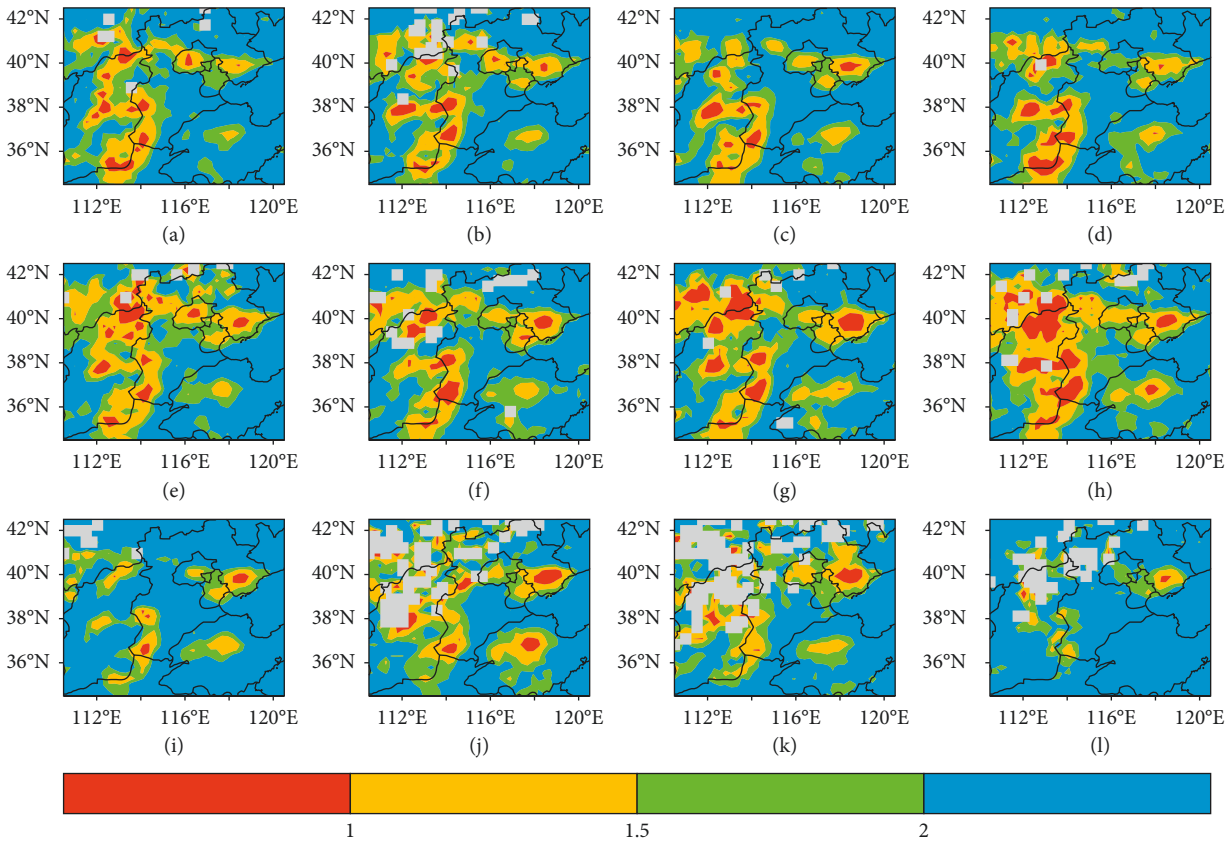

Figure 6: Average tropospheric FNR in JJA for 2005–2016. (a) 2005, (b) 2006, (c) 2007, (d) 2008, (e) 2009, (f) 2010, (g) 2011, (h) 2012, (i) 2013, (j) 2014, (k) 2015, and (l) 2016. FNR is defined as the ratio of tropospheric HCHO column concentration to tropospheric NO_2 column concentration.

surface O_3 (e.g., 8-hour max) because it directly affects human health.

3.5. Summer O_3 Fraction of Explained Variation. The fraction of explained variation is from adjusted R square in the multiple regression model formula (3). It is a change caused by other variables. The multivariate linear regression model described above was used to calculate the fraction of explained variation of the trend observed by OMI/MLS in the tropospheric O_3 for the summer season (JJA) of the entire period from 2005 to 2016. We applied the model to the

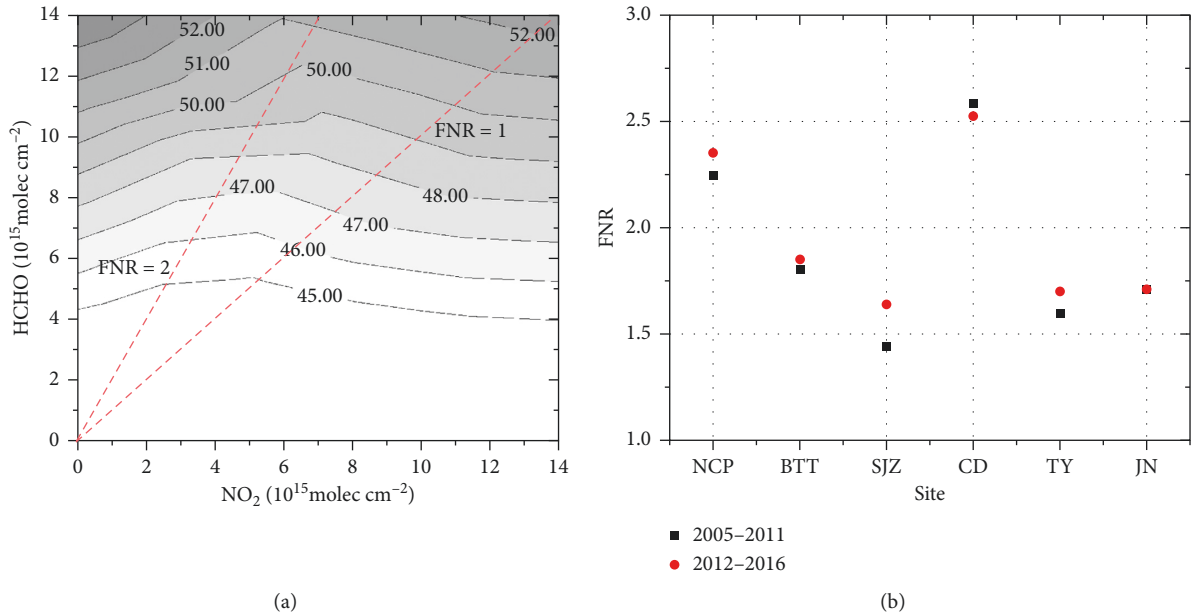

Figure 7: (a) Regional ozone-NO_x-VOC sensitivity characteristics in summer in the NCP. The contours are the tropospheric O_3 column concentrations (units: DU). (b) Comparison of FNR in major cities for two phases (2005–2011 and 2012–2016) from remote sensing. FNR is defined as the ratio of tropospheric HCHO column concentration to tropospheric NO_2 column concentration.

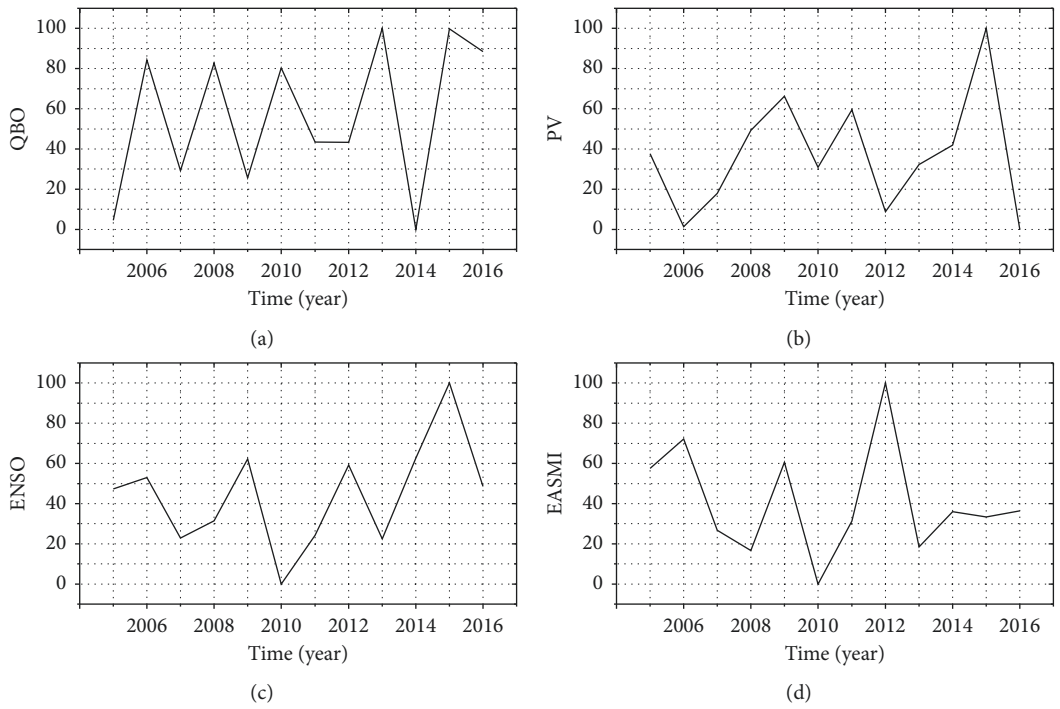

Figure 8: Annual normalized time series of (a) QBO, (b) PV, (c) ENSO, (d) and EASMI (black solid line).

variables in sequence to identify the variables that were significant for tropospheric O_3.

During the entire period of 2005–2016, the significant variables included NO_2, HCHO, CO, the QBO, the potential vorticity (PV) at 300 hPa, the ENSO index, and EASMI (Figure 8). We divided these variables into two types: atmospheric chemistry factors (NO_2, HCHO, and CO) and atmospheric dynamics factors (QBO, PV at 300 hPa, the ENSO index, and EASMI). The regression model was applied again to the atmospheric chemistry factors, and the significance of their regression fittings was in the order of $NO_2 > CO > HCHO$. The first significant variable we found

Table 2: The sum of squared residuals and the fraction of explained variation to the tropospheric O_3.

	Variables included in the fitting	SSE	Contribution to O_3 (%)
	Trend	10.93	
Emission	NO_2	7.27	69.73
	NO_2 + CO	7.10	66.75
	NO_2 + CO + HCHO	6.82	63.50
Circulation	ENSO	10.16	57.69
	ENSO + PV	9.26	56.63
	ENSO + PV + EASMI	7.35	60.64
	ENSO + PV + EASMI + QBO	7.15	55.32

for this period was the monthly NO_2. The NO_2 variable, the stable state of NO_x, is considered to be a proxy for large-scale emission changes that may affect O_3 regionally, and NO_2 could explain 69.73% of the initial trend (Table 2). CO represents a regional change in emissions due to its longer life cycle to some extent. CO could explain 60.14% of the initial trend. HCHO is an intermediate product of VOCs, and they are closely related. HCHO could explain 54.73% of the initial trend. Their overall contribution was 63.50%.

Contribution to O_3 is defined by the adjusted R square of the multivariate regression model. SSE is the sum of squared residuals (SSE). Because as the number of variables increases, R square will inevitably increase, and the accuracy cannot be truly quantified. Looking at R square alone does not infer whether the added features make sense, so here we applied adjusted R square instead of R square. When a variable is added, if this variable is meaningful, adjusted R square will increase. If this feature is redundant, adjusted R square will decrease, so the combined contribution of NO_2, CO, and HCHO to O_3 is lower than the contribution of NO_2 alone, which indicates the change of NO2 plays a leading role in the variation of O_3, and the information of the other two substances is covered by NO_2. This analysis is also applied to atmospheric circulation.

The effects of atmospheric circulation on tropospheric O_3 are characterized by the atmospheric dynamic factors: the QBO, the potential vorticity (PV) at 300 hPa, the ENSO index, and EASMI. Similar to the atmospheric chemistry factors, the regression model was also applied to the dynamic factors in sequence for another residual trend. The significance of the regression fittings of the dynamics factors was in the order of ENSO > PV > EASMI > QBO. The ENSO index showed high significance ($P = 0.0084$) for this period, which could explain 57.69% of the initial trend. The normalized ENSO index experienced an increase over the second phase (2012–2016) with strong El Niño events in 2015–2016 (Figure 8). PV reflects the height of the troposphere, and it could explain 55.79% of the initial trend. EASMI represents the intensity of the airflow between the continent and ocean. The effect of horizontal airflow could explain 54.72% of the initial trend. QBO reflects the contribution of O_3 exchange between the troposphere and the stratosphere; the vertical transport can explain 54.61% of the initial trend. Their overall contribution to the observed trend was 55.32%. The above results show that it is meaningful to add EASMI, and ENSO covers the PV information.

4. Conclusions

Satellite observations are applied to study the variability of O_3 in the troposphere in the NCP. The data used in this study combine the advantages of satellite nadir observation and limb observation modes; the nadir mode facilitates observation of the total column, and the limb mode facilitates observation of the vertical profile. Evaluation of the MLS/OMI observations has shown that the tropospheric O_3 trends seem reliable fairly and can be used to study the tropospheric O_3 trend over the NCP.

Based on long-term statistics, the tropospheric O_3 in the NCP is highest in summer (from June to August). In contrast, the O_3 content is lowest during the winter period (from December to February). Summer tropospheric O_3 column concentrations increased at an average rate of 0.55 DU/year in the NCP from 2005 to 2016.

Spatiotemporal variations of several key atmospheric components are analyzed to evaluate their impacts on O_3 formation in summer. Major air pollutants showed a trend from increasing in the first phase (2005–2011) to decreasing in the second phase (2012–2016) because of the implementation of emission reduction measures. Due to the reduction of nitrogen oxides, the NCP has been experiencing the transition of O_3-NO_x-VOC sensitivity from the NO_x-saturated state to the NO_x-limited state. However, NO_x is still saturated in megacities.

A multivariate linear regression model is applied to identify the processes driving the observed trend of summer tropospheric O_3. The contribution of atmospheric chemistry is 63.50%. The first significant variable is NO_2, and it can explain 69.73% of the initial trend. The ENSO also shows the high significance for this period, and it can explain 57.69% of the initial trend. The contribution of large-scale dynamical processes to the observed trend is 55.32%. The results suggest that both large-scale dynamical processes and regional emissions affect the interannual tropospheric O_3 variation in summer.

Our results indicate that chemical processes had a more important impact on interannual tropospheric O3 than dynamic processes. This is also reflected by other research results. The summer tropospheric O3 presented a growth trend with the growth rate of 1.28 DU·per decade over the North China Plain (NCP) for the period of 1979–2013 mainly due to increased NO_x and VOC emissions [56]. Significant increasing trends of tropospheric O_3 are also found for all seasons except for winter, with a maximum rate

of 1.10 DU·per decade for summer during 1979–2005. They do not consider atmospheric circulations to be a major factor in the tropospheric O_3 increasing trend over NCP [57].

Remote sensing data could provide long-term characteristics. It is difficult for the atmospheric chemical transport model due to emission uncertainty and limitation of computing resource [58]. However, the statistical relationship is not completely deterministic, although the results selected have passed the significance test, so we regard our conclusion as a hypothesis, which needs to be validated by a 3D model with atmospheric chemistry and meteorology that can provide mechanism analysis. The conclusion based on remote sensing data in this study is very macroscopic, and some details require further separate research. In addition, specific vertical distribution, convection processes, long-range transport, and chemical nonlinear processes require an atmospheric chemical transport model for sensitivity experiments to quantify its effects [59].

Data Availability

Data sources and links are listed in the data introduction section.

Conflicts of Interest

The authors declare that there are no conflicts of interest regarding the publication of this paper.

Acknowledgments

The authors are grateful to all the organizations and individuals who provided the data. Lihua Zhou acknowledges the financial support from the China Scholarship Council. This research was funded by the National Key R&D Program of China (grant no. 2017YFA0603603), National Science Foundation of China (grant no. 41575144), the Fundamental Research Funds for the Central Universities (grant no. 312231103), and Natural Science Foundation of China and Hong Kong Federation of Trade Unions (NSFC-RGC) (grant no. 403331160396).

References

[1] M. P. McCormick, R. E. Veiga, and W. P. Chu, "Stratospheric ozone profile and total ozone trends derived from the SAGE I and SAGE II data," *Geophysical Research Letters*, vol. 19, no. 3, pp. 269–272, 1992.

[2] F. Pacifico, G. A. Folberth, S. Sitch et al., "Biomass burning related ozone damage on vegetation over the amazon forest: a model sensitivity study," *Atmospheric Chemistry and Physics*, vol. 15, no. 5, pp. 2791–2804, 2015.

[3] X. Yue and N. Unger, "The Yale Interactive terrestrial Biosphere model version 1.0: description, evaluation and implementation into NASA GISS ModelE2," *Geoscientific Model Development*, vol. 8, no. 8, pp. 2399–2417, 2015.

[4] V. T. F. Cheung and T. Wang, "Observational study of ozone pollution at a rural site in the Yangtze Delta of China," *Atmospheric Environment*, vol. 35, no. 29, pp. 4947–4958, 2001.

[5] Y. N. Zhang, Y. R. Xiang, L. Y. Chan et al., "Procuring the regional urbanization and industrialization effect on ozone pollution in Pearl River Delta of Guangdong, China," *Atmospheric Environment*, vol. 45, no. 21, pp. 4898–4906, 2011.

[6] K. Lu, Y. Zhang, H. Su et al., "Oxidant ($O_3 + NO_2$) production processes and formation regimes in Beijing," *Journal of Geophysical Research: Atmospheres*, vol. 115, no. D7, Article ID D07303, 2010.

[7] Y. Cui, J. Lin, C. Song et al., "Rapid growth in nitrogen dioxide pollution over Western China, 2005–2013," *Atmospheric Chemistry and Physics*, vol. 16, no. 10, pp. 6207–6221, 2016.

[8] W. W. Verstraeten, J. L. Neu, J. E. Williams, K. W. Bowman, J. R. Worden, and K. F. Boersma, "Rapid increases in tropospheric ozone production and export from China," *Nature Geoscience*, vol. 8, no. 9, pp. 690–695, 2015.

[9] T. Wang, A. Ding, and J. Gao, "Strong ozone production in urban plumes from Beijing, China," *Geophysical Research Letters*, vol. 33, no. 28, Article ID L21806, 2006.

[10] J. Li, K. Lu, W. Lv et al., "Fast increasing of surface ozone concentrations in Pearl River Delta characterized by a regional air quality monitoring network during 2006–2011," *Journal of Environmental Sciences*, vol. 26, no. 1, pp. 23–36, 2014.

[11] G. Tang, X. Li, Y. Wang, J. Xin, and X. Ren, "Surface ozone trend details and interpretations in Beijing," *Atmospheric Chemistry and Physics*, vol. 9, no. 22, pp. 8813–8823, 2009.

[12] Z. Ma, J. Xu, W. Quan, Z. Zhang, W. Lin, and X. Xu, "Significant increase of surface ozone at a rural site, north of eastern China," *Atmospheric Chemistry and Physics*, vol. 16, no. 6, pp. 3969–3977, 2016.

[13] J.-B. Lee, J.-S. Cha, S.-C. Hong et al., "Projections of summertime ozone concentration over East Asia under multiple IPCC SRES emission scenarios," *Atmospheric Environment*, vol. 106, pp. 335–346, 2015.

[14] M. Li, Q. Zhang, J. Kurokawa et al., "Mix: a mosaic Asian anthropogenic emission inventory for the mics-asia and the htap projects," *Atmospheric Chemistry and Physics Discussions*, vol. 15, no. 23, pp. 34813–34869, 2015.

[15] E. R. Carrillo-Torres, I. Y. Hernández-Paniagua, and A. Mendoza, "Use of combined observational and model-derived photochemical indicators to assess the O_3-NO_x-VOC system sensitivity in urban areas," *Atmosphere*, vol. 8, no. 12, p. 22, 2017.

[16] A. H. Souri, Y. Choi, W. Jeon, J. H. Woo, Q. Zhang, and J. i. Kurokawa, "Remote sensing evidence of decadal changes in major tropospheric ozone precursors over East Asia," *Journal of Geophysical Research: Atmospheres*, vol. 122, no. 4, pp. 2474–2492, 2017.

[17] X. Xie, M. Shao, Y. Liu, S. Lu, C.-C. Chang, and Z.-M. Chen, "Estimate of initial isoprene contribution to ozone formation potential in Beijing, China," *Atmospheric Environment*, vol. 42, no. 24, pp. 6000–6010, 2008.

[18] M. Shao, S. Lu, Y. Liu et al., "Volatile organic compounds measured in summer in Beijing and their role in ground-level ozone formation," *Journal of Geophysical Research*, vol. 114, no. D2, Article ID D00G06, 2009.

[19] J. L. An, Y. S. Wang, F. K. Wu, and Z. Bin, "Characterizations of volatile organic compounds during high ozone episodes in Beijing, China," *Environmental Monitoring and Assessment*, vol. 184, no. 4, pp. 1879–1889, 2012.

[20] J. Duan, J. Tan, L. Yang, S. Wu, and J. Hao, "Concentration, sources and ozone formation potential of volatile organic compounds (VOCs) during ozone episode in Beijing," *Atmospheric Research*, vol. 88, no. 1, pp. 25–35, 2008.

[21] X. Jin and T. Holloway, "Spatial and temporal variability of ozone sensitivity over China observed from the Ozone Monitoring Instrument," *Journal of Geophysical Research: Atmospheres*, vol. 120, no. 14, pp. 7229–7246, 2015.

[22] H. Irie, Y. Kanaya, H. Akimoto et al., "Validation of OMI tropospheric NO_2 column data using MAX-DOAS measurements deep inside the north China plain in June 2006: mount tai experiment 2006," *Atmospheric Chemistry and Physics*, vol. 8, no. 22, pp. 6577–6586, 2008.

[23] X. Zhang, H. Jiang, X. Lu et al., "Estimate of methane release from temperate natural wetlands using Envisat/Sciamachy data in China," *Atmospheric Environment*, vol. 69, pp. 191–197, 2013.

[24] N. A. Krotkov, C. A. Mclinden, C. Li et al., "Aura OMI observations of regional SO_2 and NO_2 pollution changes from 2005 to 2015," *Atmospheric Chemistry and Physics*, vol. 16, no. 7, pp. 4605–4629, 2016.

[25] K. F. Boersma, D. J. Jacob, H. J. Eskes, R. W. Pinder, J. Wang, and A. J. van der Ronald, "Intercomparison of SCIAMACHY and OMI tropospheric NO_2 columns: observing the diurnal evolution of chemistry and emissions from space," *Journal of Geophysical Research Atmospheres*, vol. 113, no. D16, Article ID D16S26, 2008.

[26] K. F. Boersma, D. J. Jacob, M. Trainic et al., "Validation of urban NO_2 concentrations and their diurnal and seasonal variations observed from the SCIAMACHY and OMI sensors using in situ surface measurements in Israeli cities," *Atmospheric Chemistry and Physics*, vol. 9, no. 12, pp. 3867–3879, 2009.

[27] J. Fishman, C. E. Watson, J. C. Larsen, and J. A. Logan, "Distribution of tropospheric ozone determined from satellite data," *Journal of Geophysical Research*, vol. 95, no. D4, Article ID 3599, 1990.

[28] J. Fishman, V. G. Brackftt, and K. Fakhruzzaman, "Distribution of tropospheric ozone in the tropics from satellite and ozonesonde measurements," *Journal of Atmospheric and Terrestrial Physics*, vol. 54, no. 5, pp. 589–597, 1992.

[29] J. R. Ziemke, S. Chandra, B. N. Duncan et al., "Tropospheric ozone determined from aura OMI and MLS: evaluation of measurements and comparison with the global modeling initiative's chemical transport model," *Journal of Geophysical Research Atmospheres*, vol. 111, no. D19, Article ID D19303, 2006.

[30] J. R. Ziemke, S. Chandra, G. J. Labow, P. K. Bhartia, L. Froidevaux, and J. C. Witte, "A global climatology of tropospheric and stratospheric ozone derived from Aura OMI and MLS measurements," *Atmospheric Chemistry and Physics*, vol. 11, no. 17, pp. 17879–17911, 2011.

[31] L.-H. Zhou, X.-Y. Zhang, J. Zhang, S.-G. Zhu, and X.-Y. Meng, "A case study of air quality control in Beijing and the surrounding area during the 2015 World Championships and Parade," *Atmospheric and Oceanic Science Letters*, vol. 10, no. 3, pp. 252–260, 2017.

[32] K. Huang, X. Zhang, and Y. Lin, "The "APEC Blue" phenomenon: regional emission control effects observed from space," *Atmospheric Research*, vol. 164-165, no. 165, pp. 65–75, 2015.

[33] L. Zhu, D. J. Jacob, L. J. Mickley et al., "Anthropogenic emissions of highly reactive volatile organic compounds in eastern Texas inferred from oversampling of satellite (OMI) measurements of HCHO columns," *Environmental Research Letter*, vol. 9, no. 11, Article ID 114004, 2014.

[34] B. A. Gray, Y. Wang, D. Gu et al., "Sources, transport, and sinks of SO_2 over the equatorial pacific during the pacific atmospheric sulfur experiment," *Journal of Atmospheric Chemistry*, vol. 68, no. 1, pp. 27–53, 2011.

[35] C. L. Heald, D. J. Jacob, A. M. Fiore et al., "Asian outflow and trans-Pacific transport of carbon monoxide and ozone pollution: an integrated satellite, aircraft, and model perspective," *Journal of Geophysical Research: Atmospheres*, vol. 108, no. D24, Article ID 4804, 2003.

[36] G. Dufour, M. Eremenko, M. Beekmann et al., "Lower tropospheric ozone over the North China Plain: variability and trends revealed by IASI satellite observations for 2008–2016," *Atmospheric Chemistry and Physics*, vol. 18, no. 22, pp. 16439–16459, 2018.

[37] S. K. Panda and P. K. Jana, "Uncertainty-based QoS min-min algorithm for heterogeneous multi-cloud environment," *Arabian Journal for Science and Engineering*, vol. 41, no. 8, pp. 3003–3025, 2016.

[38] H. Cao, J. Liu, G. Wang, G. Yang, and L. Luo, "Identification of sand and dust storm source areas in Iran," *Journal of Arid Land*, vol. 7, no. 5, pp. 1415–1418, 2015.

[39] J. Li and Q. Zeng, "A unified monsoon index," *Geophysical Research Letters*, vol. 29, no. 8, p. 115, 2002.

[40] J. Li and Q. Zeng, "A new monsoon index and the geographical distribution of the global monsoons," *Advances in Atmospheric Sciences*, vol. 20, no. 2, pp. 299–302, 2003.

[41] J. Li and Q. Zeng, "A new monsoon index, its interannual variability and relation with monsoon precipitation," *Climatic and Environmental Research*, vol. 10, no. 3, pp. 351–365, 2005.

[42] B. N. Duncan, Y. Yoshida, J. R. Olson et al., "Application of OMI observations to a space-based indicator of NO_x and VOC controls on surface ozone formation," *Atmospheric Environment*, vol. 44, no. 18, pp. 2213–2223, 2010.

[43] X. Jin, A. M. Fiore, L. T. Murray et al., "Evaluating a space-based indicator of surface ozone-NOx-VOC sensitivity over midlatitude source regions and application to decadal trends," *Journal of Geophysical Research: Atmospheres*, vol. 122, no. 19, pp. 10439–10461, 2017.

[44] G. Verstraeten, L. Baeten, T. Van den Broeck et al., "Temporal changes in forest plant communities at different site types," *Applied Vegetation Science*, vol. 16, no. 2, pp. 237–247, 2013.

[45] S. S. Brown, H. Stark, T. B. Ryerson et al., "Nitrogen oxides in the nocturnal boundary layer: simultaneous in situ measurements of NO_3, N_2O_5, NO_2, NO, and O_3," *Journal of Geophysical Research: Atmospheres*, vol. 108, no. D9, Article ID 4299, 2003.

[46] B. D. Foy, Z. Lu, D. G. Streets, L. N. Lamsal, and B. N. Duncan, "Estimates of power plant NO_x, emissions and lifetimes from OMI NO_2 satellite retrievals," *Atmospheric Environment*, vol. 116, pp. 1–11, 2015.

[47] Z.-H. Shon, S. Madronich, S.-K. Song et al., "Characteristics of the NO-NO_2-O_3 system in different chemical regimes during the MIRAGE-Mex field campaign," *Atmospheric Chemistry and Physics*, vol. 8, no. 23, pp. 7153–7164, 2008.

[48] D. Gu, Y. Wang, C. Smeltzer, and K. F. Boersma, "Anthropogenic emissions of NO_x over China: reconciling the difference of inverse modeling results using GOME-2 and OMI measurements," *Journal of Geophysical Research: Atmospheres*, vol. 119, no. 12, pp. 7732–7740, 2014.

[49] S. Xie, T. Yu, Y. Zhang, L. Zeng, L. Qi, and X. Tang, "Characteristics of PM10, SO_2, NO_x and O_3 in ambient air during the dust storm period in Beijing," *Science of the Total Environment*, vol. 345, no. 1–3, pp. 153–164, 2005.

[50] Z. Jiang, J. R. Worden, H. Worden et al., "A 15-year record of CO emissions constrained by MOPITT CO observations,

Atmospheric Chemistry and Physics," *Mechanical Engineering Faculty Contributions*, vol. 17, no. 7, pp. 4565–4583, 2017.

[51] B. Zheng, F. Chevallier, P. Ciais et al., "Rapid decline in carbon monoxide emissions and export from East Asia between years 2005 and 2016," *Environmental Research Letters*, vol. 13, no. 4, Article ID 044007, 2018.

[52] H. Liu, D. J. Jacob, I. Bey, R. M. Yantosca, B. N. Duncan, and G. W. Sachse, "Transport pathways for Asian pollution outflow over the pacific: interannual and seasonal variations," *Journal of Geophysical Research*, vol. 108, no. D20, Article ID 8786, 2003.

[53] J. Fishman and W. Seiler, "Correlative nature of ozone and carbon monoxide in the troposphere: implications for the tropospheric ozone budget," *Journal of Geophysical Research*, vol. 88, no. C6, pp. 3662–3670, 1983.

[54] M. Chin, D. J. Jacob, J. W. Munger, D. D. Parrish, and B. G. Doddridge, "Relationship of ozone and carbon monoxide over North America," *Journal of Geophysical Research*, vol. 99, no. D7, pp. 14565–14573, 1994.

[55] S. Sillman, R. Vautard, and L. Menut, "O_3-NO_x-VOC sensitivity and NO_x-VOC indicators in paris: results from models and atmospheric pollution over the paris area (ESQUIF) measurements," *Journal of Geophysical Research Atmospheres*, vol. 108, no. D17, Article ID 8563, 2003.

[56] X. Chen, X. Xia, J. Cao, F. Huang, and X. Xu, "Analysis of long-term trend of tropospheric ozone in north china and its impact factors," *Chinese Science Bulletin*, vol. 60, no. 27, pp. 2659–2666, 2015.

[57] X. Xu and W. Lin, "Trends of tropospheric ozone over China based on satellite data (1979-2005)," *Advances in Climate Change Research*, vol. 2, no. 1, pp. 43–48, 2011.

[58] J. Xing, S. X. Wang, C. Jang, Y. Zhu, and J. M. Hao, "Nonlinear response of ozone to precursor emission changes in China: a modeling study using response surface methodology," *Atmospheric Chemistry and Physics*, vol. 11, no. 10, pp. 5027–5044, 2011.

[59] H.-D. Choi, H. Liu, J. H. Crawford et al., "Global O3-CO correlations in a chemistry and transport model during July-August: evaluation with TES satellite observations and sensitivity to input meteorological data and emissions," *Atmospheric Chemistry and Physics*, vol. 17, no. 13, pp. 8429–8452, 2017.